Robust Digital Watermarking in the Ridgelet Domain

Patrizio Campisi, *Member, IEEE*, Deepa Kundur, *Senior Member, IEEE*, and Alessandro Neri, *Member, IEEE*

***Abstract*—In this letter, we propose a multiplicative watermarking method operating in the ridgelet domain. We employ the directional sensitivity and the anisotropy of the ridgelet transform (RT) in order to obtain a sparse image representation, where the most significant coefficients represent the most energetic direction of an image with straight edges. Therefore, given a natural image, the associated edge image is obtained by means of a filter bank designed using the circular harmonic functions, then the edge image is partitioned into small blocks in order to deal with straight edges. Finally, the RT is performed for each block, the most relevant coefficients are selected, and eventually the watermark is embedded. Robustness and transparency are proven by experimental results.**

***Index Terms*—Digital watermarking, ridgelet transform.**

I. Introduction

In THE RECENT past, several watermarking algorithms have used image representations where most information is concentrated into a small number of coefficients. In this fashion, watermarking methods operating in the wavelet domain [1] and in the discrete cosine transform (DCT) domain have been proposed [2], [3].

A novel approach is used in this work where we propose a watermarking method based on the use of the ridgelet transform (RT) [4]. The RT uses basis elements which exhibit high directional sensitivity and are highly anisotropic. The RT allows obtaining a sparse image representation where the most significant coefficients represent the most energetic direction of an image with straight edges. However, since edges in images are typically curved, in order to obtain an effective image representation through the RT, the image is partitioned into blocks of side-length such that an edge appears as a straight line. As a preprocessing step, we resort to extract the edge image by projecting the given image onto the domain of the circular harmonic functions (CHF) [5]. The edge image is partitioned into blocks and the RT of each block is considered. Within each block, the most significant directions are selected. Finally, the coefficients related to the selected directions are watermarked.

II. Ridgelet Transform

The RT was introduced in [4] in order to provide a sparse representation for functions defined on the continuum plane $\mathbf{R}^2$. The transform allows representing edges and other singularities along curves in a more efficient way, in terms of compactness of the representation, than traditional transformations, such as the wavelet transform, for a given accuracy of reconstruction [6]. The basic idea is to map a *line* singularity in the two-dimensional (2-D) domain into a point by means of the Radon transform [7]. Then, a one-dimensional (1-D) wavelet is performed to deal with the *point* singularity in the Radon domain.

In Section II-A, the continuous RT (CRT) is defined. However for practical applications a discrete implementation of the RT is necessary. In Section II-B, we briefly summarize the implementation of the finite RT that was proposed in [8].

A. CRT

Let us indicate with $\psi(\cdot)$ a 1-D wavelet. The elements $\psi_{(a,b,\theta)}(x_1,x_2)$ defined as

$$\psi_{(a,b,\theta)}(x_1,x_2)=a^{-\frac{1}{2}}\psi\left(\frac{(x_1\cos\theta+x_2\sin\theta-b)}{a}\right) \quad (1)$$

where $a>0$ is a scale parameter and (θ,b) are the parameters of the line $x_1\cos\theta+x_2\sin\theta=b$ are the so-called ridgelets. Since a generic cross section of (1) is constant along the line (ridge) $x_1\cos\theta+x_2\sin\theta=b$ and the cross section along the orthogonal direction is a wavelet, the ridgelets can be thought as a concatenation of 1-D wavelets along lines.

Therefore, the ridgelets seem to be good candidates to provide a parsimonious representation of natural images which are composed by objects with singularities along lines.

Given an integrable function $f(x_1,x_2)$ in $\mathbf{R}^2$, its CRT is defined as [6]

$$\mathrm{CRT}_f(a,b,\theta)=\int_{\mathbf{R}^2}\psi_{(a,b,\theta)}(x_1,x_2)f(x_1,x_2)dx_1dx_2. \quad (2)$$

The reconstruction formula is given by the following [6]:

$$f(x_1,x_2)=\int_0^{2\pi}\int_{-\infty}^{\infty}\int_0^{\infty}\mathrm{CRT}_f(a,b,\theta)\psi_{(a,b,\theta)}(x_1,x_2)\frac{da}{a^3}db\frac{d\theta}{4\pi}.$$

The CRT, defined by (1) and (2), can be evaluated by performing the wavelet analysis in the Radon domain. Specifically, let us recall that the Radon transform is defined as

$$R_f(\theta,t)=\int_{\mathbf{R}^2}f(x_1,x_2)\delta(x_1\cos\theta+x_2\sin\theta-t)dx_1dx_2$$

being $(\theta,t)\in[0,2\pi)\times\mathbf{R}$ and δ the Dirac distribution. The CRT is then obtained by applying a 1-D wavelet transform to $R_f(\theta,t)$ as follows:

$$\mathrm{CRT}_f(a,b,\theta)=a^{-\frac{1}{2}}\int_{\mathbf{R}}\psi\left(\frac{t-b}{a}\right)R_f(\theta,t)dt.$$

Manuscript received December 25, 2003; revised March 9, 2004. The associate editor coordinating the review of this manuscript and approving it for publication was Dr. Dipti Prasad Mukherjee.

P. Campisi and A. Neri are with the Dipartmento di Elettronica Applicata, Universitá degli Studi Roma Tre, I-00146 Roma, Italy (e-mail: campisi@uniroma3.it; neri@uniroma3.it).

D. Kundur is with the Department of Electrical Engineering, Texas A&M University, College Station, TX 77843-3128 USA (e-mail: deepa@ee.tamu.edu).

Digital Object Identifier 10.1109/LSP.2004.835463

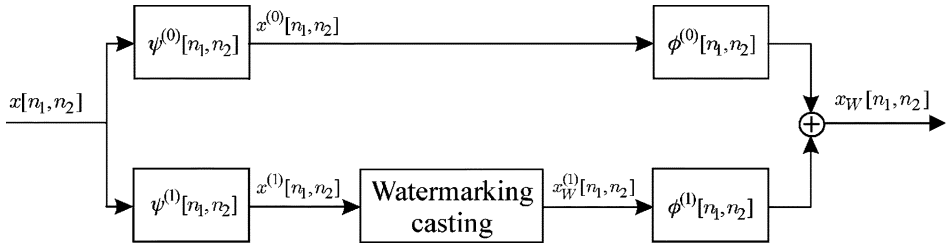

Fig. 1. Proposed watermarking system.

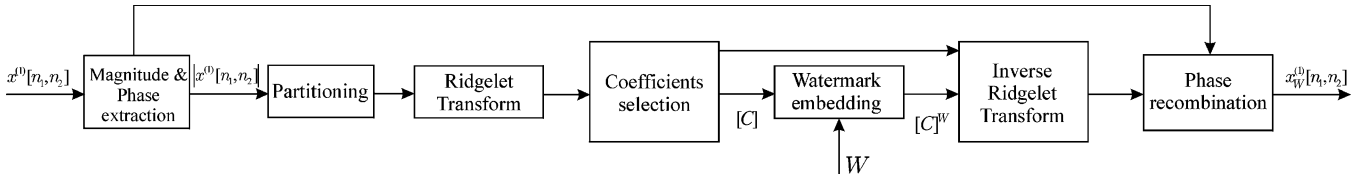

Fig. 2. Watermark casting.

B. Digital RT

In [8], a finite Radon transform (FRAT) is introduced. The FRAT of a real function f defined on a finite grid Z_p^2, being $Z_p = \{0, 1, \ldots, p-1\}$ where p is a prime number, is

$$r_k[l] = \mathrm{FRAT}_f(k,l) = \frac{1}{\sqrt{p}} \sum_{(i,j)\in L_{k,l}} f[i,j].$$

$L_{k,l}$ defines the set of points that form a line on the lattice Z_p^2. Specifically

$$L_{k,l} = \{(i,j) : j = ki + l \ (\mathrm{mod}\ p), i \in Z_p\}$$
$$L_{p,l} = \{(l,j) : j \in Z_p\}$$

being $0 \le k < p$ the line direction (where $k = p$ corresponds to the vertical line) and l its intercept. In [8], it has been demonstrated that FRAT is invertible, thus providing a representation for a generic image. The invertible finite RT $\mathrm{FRIT}_f[k,q]$, with $q \in Z_p$, is obtained by taking the 1-D discrete wavelet transform on each FRAT projection sequence $r_k[0], r_k[1], \ldots, r_k[p-1]$, for each direction k.

III. Proposed Watermarking System

In order to perform the embedding of the mark, we resort to represent the host image by means of a suitable subband decomposition. Specifically, we project the image onto the domain of the CHFs [5], thus obtaining complex valued images, whose magnitude reveals the presence of specific features, and the phase measures their orientation. The CHF we have used in this letter are expressed by the separable continuous functions

$$\psi^{(n)}(r,\theta) = r^n e^{-r^2} e^{-jn\theta} \tag{3}$$

with $n = 0, 1, 2, 3, \ldots$, known as "marginal" Hermite filters. Specifically, the nth-order CHF is tuned to the fundamental harmonics of n-fold angular symmetric patterns, corresponding to edges ($n = 1$), lines ($n = 2$), forks ($n = 3$), crosses ($n = 4$), and so on. As detailed in Section III-A, in our application we choose to decompose the image by means of a filter pair belonging to the class of the CHF composed by a low-pass filter and by a first-order filter whose output captures the image's edges (see Fig. 1). Then, as described in Section III-B, a compact representation of the magnitude of the edge image is carried out in the Ridgelet domain. Specifically, with reference to Fig. 2, the edge image is first partitioned into blocks whose width is such that a curved edge appears to be straight. Then the RT is performed on each block. For each block, the direction having the greater energy is selected. After having collected the coefficients representing the most significant direction of each block they are marked with a random generated mark. The inverse RT is finally performed, thus obtaining the marked magnitude of the edge image.

A. Image Representation in the CHF Domain

With reference to Fig. 1, the image $x[n_1, n_2]$, is passed through a filter pair composed by the low-pass filter $\psi^{(0)}[n_1, n_2]$ and a bandpass filters $\psi^{(1)}[n_1, n_2]$ whose impulse responses are a discrete implementation of (3) and are expressed by

$$\begin{cases} \psi^{(0)}[n_1,n_2] = e^{-\frac{r^2[n_1,n_2]}{\sigma_0^2}} \\ \psi^{(1)}[n_1,n_2] = \frac{r[n_1,n_2]}{\sigma_1} e^{-\frac{r^2[n_1,n_2]}{\sigma_1^2}} e^{-j\theta[n_1,n_2]} \end{cases} \tag{4}$$

where $r[n_1,n_2] \stackrel{\mathrm{def}}{=} \sqrt{n_1^2+n_2^2}$ and $\theta \stackrel{\mathrm{def}}{=} \arctan n_1/n_2$ are discrete polar pixel coordinates. The selectivity of the filters in (4) is determined by the form factors σ_0 and σ_1. By denoting with $\Psi^{(i)}(e^{j\omega_1}, e^{j\omega_2})$ the bidimensional Fourier transform of $\psi^{(i)}[n_1, n_2]$, with $i = 0, 1$, we obtain

$$\begin{cases} \Psi^{(0)}(e^{j\omega_1}, e^{j\omega_2}) \simeq \pi\sigma_0^2 e^{-\frac{\rho^2(\omega_1,\omega_2)\sigma_0^2}{4}} \\ \Psi^{(1)}(e^{j\omega_1}, e^{j\omega_2}) \simeq \frac{-j\pi\sigma_1^3}{2} \rho(\omega_1,\omega_2) e^{-\frac{\rho^2(\omega_1,\omega_2)\sigma_1^2}{4}} e^{-j\gamma(\omega_1,\omega_2)} \end{cases}$$

being $\rho(\omega_1,\omega_2) \stackrel{\mathrm{def}}{=} \sqrt{\omega_1^2+\omega_2^2}$, and $\gamma(\omega_1,\omega_2) \stackrel{\mathrm{def}}{=} \arctan \omega_2/\omega_1$ the polar coordinates in the spatial radian frequency domain.

The zero-order circular harmonic filter $\psi^{(0)}[n_1, n_2]$ extracts a low-pass version of the input image; the form factor σ_0 is chosen so as to retain only very low spatial frequencies. The first-order circular harmonic filter $\psi^{(1)}[n_1, n_2]$ is a bandpass filter, with frequency selectivity set by properly choosing the form factor σ_1. The output of this filter is a complex image $x^{(1)}[n_1, n_2]$ whose

magnitude reveals the presence of edges and whose phase is proportional to their orientation. The magnitude of $x^{(1)}[n_1, n_2]$ is then marked as detailed in Section III-B.

B. Watermark Embedding

Given the edge image $x^{(1)}[n_1, n_2]$, obtained as detailed in Section III-A, its magnitude is partitioned into B blocks $x_h^{(1)}[n_1, n_2]$, with $h = 1, 2, \ldots, B$, of $N \times N$ pixels. The partition is done in such a way that a curved edge in the edge image is represented as segments of line in some adjacent blocks. This is done because, as pointed out in [8], discrete ridgelet representation allows tackling the problem of approximation of smooth regions having straight edges. As an embedding criterion, we resort to embed the watermark in the most energetic edges of the image. The rationale behind this approach relies on the fact that, in order to design a robust watermarking method, the mark has to be embedded into perceptually significant features of an image, such as edges. In this fashion, attacks which try to destroy the mark, are likely to severely affect the features where the mark has been embedded thus making the host data unusable after the attack.

Specifically, for each block $x_h^{(1)}[n_1, n_2]$ the finite RT $\mathrm{FRIT}_{x_h^{(1)}}[k, q]$ is computed, thus obtaining the ridgelet coefficients for the directions $0 \leq k \leq p$, with $p = N$. Then, within the block h, the direction $\overline{k}_h$ having the higher energy with respect to the others, that is

$$\overline{k}_h = \max_k \left(\frac{1}{p} \sum_{q=0}^{p-1} \left(\mathrm{FRIT}_{x_h^{(1)}}[k, q] \right)^2 \right) \tag{5}$$

is selected. The ridgelet coefficients $\mathrm{FRIT}_{x_h^{(1)}}[\overline{k}_h, q]$, with $q = 0, 1, \ldots, p-1$, corresponding to the selected direction $\overline{k}_h$, are the representation of the most energetic edge in the hth block; therefore, they are the coefficients to be marked according to the approach proposed.

The selection of the most relevant direction is iterated for each block, and their respective ridgelet coefficients are collected in the vectors $\mathbf{v}_h$, with $h = 1, 2, \ldots, B$. The ridgelets coefficients matrix $[C] = [\mathbf{v}_1, \mathbf{v}_2, \ldots, \mathbf{v}_B] = \{c_{ij}\}$, with $i = 1, 2, \ldots, N$ and $j = 1, 2, \ldots, B$, is then constructed. Then, the watermark $W = \{w_1, w_2, \ldots, w_B\}$, whose values are determinations of a random variable having normal distribution, zero mean, and unit variance, is superimposed onto each row i of the matrix $[C]$ according to the following law:

$$c_{ij}^W = c_{ij} + \alpha |c_{ij}| w_j$$

with $j = 1, 2, \ldots, B$ and α the watermark power factor. The watermarked ridgelet coefficients matrix $[C]^W = [\mathbf{v}_1^W, \mathbf{v}_2^W, \ldots, \mathbf{v}_B^W]$ is thus obtained. Roughly speaking, the same watermark coefficient is embedded into each ridgelet coefficient of the most representative direction of the block under analysis, which improves the robustness of the method.

Then the watermarked coefficients are inserted back in the same locations where they have been taken from and the inverse RT is performed. Once the magnitude of the edge image is watermarked, it is combined with the phase of the unmarked edge image thus leading to the watermarked edge image $x_W^{(1)}[n_1, n_2]$. Eventually, the reconstructed watermarked image is obtained as specified in Section III-C.

C. Image Reconstruction

Given the circular harmonic components $x^{(0)}[n_1, n_2]$ and $x_W^{(1)}[n_1, n_2]$ which host the mark, the watermarked image is obtained through a suitable inverse filter-bank (Fig. 1), namely

$$x_W[n_1, n_2] = \left(\phi^{(0)} * x^{(0)} \right)[n_1, n_2] + \left(\phi^{(1)} * x_W^{(1)} \right)[n_1, n_2].$$

The inverse filters $\phi^{(i)}[n_1, n_2]$, with $i = 0, 1$ whose bidimensional Fourier transform are denoted with $\Psi^{(i)}(e^{j\omega_1}, e^{j\omega_2})$ must satisfy the invertibility condition. In the frequency domain, the latter is written as follows:

$$\sum_{i=0}^{1} \Psi^{(i)}(e^{j\omega_1}, e^{j\omega_2}) \cdot \Phi^{(i)}(e^{j\omega_1}, e^{j\omega_2}) = 1.$$

In particular, $\overline{(\cdot)}$ being the conjugate operator, we have chosen

$$\Phi^{(i)}(e^{j\omega_1}, e^{j\omega_2}) = \frac{\overline{\Psi^{(i)}}(e^{j\omega_1}, e^{j\omega_2})}{\left| \Psi^{(0)}(e^{j\omega_1}, e^{j\omega_2}) \right|^2 + \left| \Psi^{(1)}(e^{j\omega_1}, e^{j\omega_2}) \right|^2}.$$

IV. Watermark Detection

The watermark detection is performed by applying dual operations with respect to the ones performed for watermark embedding. Specifically, given a possibly corrupted image, the edge image is extracted as detailed in Section III-A, then its magnitude is partitioned into B blocks of dimension $N \times N$ pixels and the RT transform is performed for each block. The coefficients belonging to directions having the greatest energy within the block are selected and collected in the vectors $\mathbf{v}_h^*$, with $h = 1, 2, \ldots, B$. The extracted coefficients matrix $[C]^* = [\mathbf{v}_1^*, \mathbf{v}_2^*, \ldots, \mathbf{v}_B^*] = \{c_{ij}^*\}$, with $i = 1, 2, \ldots, N$ and $j = 1, 2, \ldots, B$, is then constructed. A correlation detector z, which evaluates the average correlation between each row of $[C]^*$ and the watermark W is taken into account

$$z = \frac{1}{N} \sum_{i=1}^{N} \left(\frac{1}{B} \sum_{j=1}^{B} c_{ij}^* w_j \right). \tag{6}$$

In case we need to determine whether the mark is present or not, z is compared to a threshold. Following the same arguments presented in [3], the threshold is set to

$$T_z = \frac{1}{N} \sum_{i=1}^{N} \left(\frac{\alpha}{3B} \sum_{j=1}^{B} c_{ij}^* \right). \tag{7}$$

Otherwise, if we have to distinguish between an ensemble of multiple marks, we can evaluate the correlation for all the marks and decide that the mark that gives the higher correlation hsa been embedded. The detector we use in this letter is optimum for additive watermark embedding and host coefficients having a Gaussian distribution. However, the watermarking technique we use is a multiplicative one and we do not make assumptions on the distribution of the ridgelet coefficients. Therefore, the detector (6) is a suboptimum one. An optimum detector and

TABLE I
PERCEPTUAL DISTORTION METRICS EVALUATION

Image	Watson's metric	PSNR (dB)
Baboon	0.002	37.6
Barbara	0.0014	40.14
Boat	0.0017	38.34
Lena	0.0013	40.46
Airplane	0.0012	38.05
Susie	0.00066	42

TABLE II
PERFORMANCES OF THE PROPOSED WATERMARKING SCHEME

Attack	Threshold Detection %	Higher Corr. Value %
Shearing ($x = 0\%, y = 1\%$)	50	70
Shearing ($x = 1\%, y = 0\%$)	70	70
JPEG2000 (0.2 bit rate)	90	100
Rotation (5 degrees)	90	100
Rotation (10 degrees)	90	100
Rotation (15 degrees)	70	90
Rotation (30 degrees)	40	80

decoder could be designed if the probability density function of the ridgelet coefficients were known.

V. EXPERIMENTAL RESULTS AND CONCLUSIONS

For our experiments we have used ten different images (Baboon, Barbara, Boat, Lena, Airplane, etc.) of dimension of 510 × 510 pixels. They have been partitioned into blocks of $N \times N$ pixels with $N = 17$, thus obtaining $B = 900$ blocks. A watermark composed by $B = 900$ elements drawn from a Gaussian distribution having zero mean and unit variance is superimposed to the data in the ridgelet domain as detailed in Section III using an embedding factor $\alpha = 0.35$. To characterize the perceptual distortion that derives from watermark embedding, we consider two different metrics that compare the original and the watermarked image: the peak signal-to-noise ratio (PSNR) and the Watson's distortion metric [10]. In Table I, the aforementioned metrics have been detailed for some of the images used in our experiments. The reported values guarantee the imperceptibility of the embedded mark. The watermark detection has been carried out by using 1000 randomly generated marks. The robustness of the proposed watermarking system has been tested against different kind of attacks using the Stirmark software [9]. For the Stirmark attacks which follow, the detector expressed by (6) provides a correlation value far higher than the threshold evaluated by means of (7) only for the actual embedded watermark out of the 1000 tested: centered cropping (1%, 2%, 5%, 10%, 15%, 20%, 25%, 50%), scaling by factors 0.5, 0.75, 0.9, 1.1, 1.5, 2, 3 × 3 median filtering, Gaussian filtering, sharpening, horizontal flip, color quantization, JPEG compression (quality factors 90, 80, 70, 60, 50, 40, 35, 30, 25, 20, 15, 10), symmetric and asymmetric line and column removal ((numbers of rows removed) = (17, 5), (1, 5), (1, 1), (5, 17), (5, 1)), aspect ratio modification ((x, y) = (80%, 100%), (90%, 100%), (100%, 80%), (100%, 90%), (100%, 110%), (100%, 120%), (120%, 100%), (110%, 100%)), rotation by a small angle (−2, −1, −0.75, −0.5, −0.25, 0.25, 0.5, 0.75, 1, and 2 degrees), and frequency mode Laplacian removal attack. All the aforementioned attacks, except for the JPEG attack itself, have been followed by a JPEG compression with quality factor of 70 and a Stirmark coefficient equal to 1 is obtained for all the ten images which have been analyzed. Moreover, the method has shown its robustness even against other attacks such as stretching, equalization, blurring, and JPEG2000 compression at 0.5, 0.4, 0.3, 0.25 bits/pixel. The method breaks down when the "Stirmark" random geometric distortions are considered. In Table II, the performances of the proposed method with respect to the Stirmark harming attacks are detailed. Specifically, the percentage of the experiments

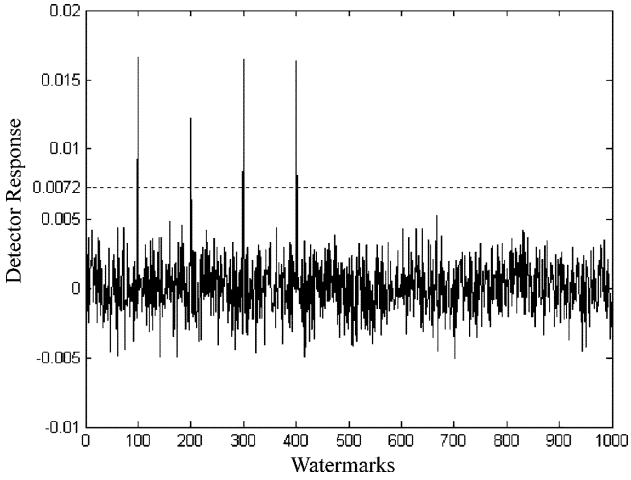

Fig. 3. Detector response for the image "Boat" with four different marks (threshold indicated by the dotted line).

where the correlation between the received data and the actual watermark is higher than the threshold ("Threshold Detection") is reported. These results refer to 1000 watermark-detection experiments for each of the ten images under analysis. Moreover, in Table II, the percentage of the experiments, averaged over the images set, where the aforementioned correlation is greater than that evaluated with other 999 tested watermarks ("Higher Corr. Value") is reported. It is evident that rotation by large angles lower the algorithm performances. This is due to the fact that because of the rotation there is no more a correspondence between the blocks of the original image and the blocks of the rotated image. Therefore, the most representative direction of one block of the rotated image does not correspond to the most representative direction of the corresponding block of the original image. A resynchronization technique would be necessary to counteract the rotation by large angles attack. Moreover, the method has been tested for multiple marks attacks. As shown in Fig. 3, that refers to the image "Boat" marked with four different marks in positions 100, 200, 300, and 400, the detector is able to retrieve all the watermarks embedded in the image out of the 1000 tested. Similar results have been obtained for the other tested images. In summary, the proposed method exhibits high robustness to most attacks, while maintaining an excellent perceptual invisibility.

REFERENCES

[1] D. Kundur and D. Hatzinakos, "Digital watermarking using multiresolution wavelet decomposition," in *Proc. ICASSP*, 1998, pp. 2969–2972.
[2] I. J. Cox, J. Kilian, F. T. Leighton, and T. Shamoon, "Secure spread spectrum watermarking for multimedia," *IEEE Trans. Image Processing*, vol. 6, pp. 1673–1687, Dec. 1997.

[3] M. Barni, F. Bartolini, V. Cappellini, and A. Piva, "A DCT-domain system for robust image watermarking," in *Signal Processing*, vol. 66, 1998, pp. 357–372.
[4] E. J. Candès and D. L. Donoho, "Ridgelets: A key to higher-dimensionality intermittency?," *Philos. Trans. R. Soc. London A*, pp. 2495–2509, 1999.
[5] G. Jacovitti and A. Neri, "Multiresolution circular harmonic decomposition," *IEEE Trans. Signal Processing*, vol. 48, pp. 3242–3247, Nov. 2000.
[6] J.-L. Starck, E. J. Candès, and D. L. Donoho, "The curvelet transform for image denoising," *IEEE Trans. Image Processing*, vol. 11, pp. 670–684, June 2002.
[7] S. R. Deans, *The Radon Trasnform and Some of Its Applications*. New York: Wiley, 1983.
[8] M. N. Do and M. Vetterli, "The finite ridgelet transform for image representation," *IEEE Trans. Image Processing*, vol. 12, pp. 16–28, Jan. 2003.
[9] F. A. P. Petitcolas, "Watermarking schemes evaluation," *IEEE Signal Processing Mag.*, vol. 17, pp. 58–64, Sept. 2000.
[10] A. B. Watson, "DCT quantization matrices optimized for indivudual images," in *Proc. SPIE, Human Vision, Visual Processing, and Digital Display IV*, vol. 1913, 1993.